Draft version April 9, 2026
Typeset using LaTeX **twocolumn** style in AASTeX631

Sparse Identification of Inviscid Fluid Dynamics from High-Dimensional Spatial-Temporal Data

Denario[1]

[1]*Anthropic, Gemini & OpenAI servers. Planet Earth.*

ABSTRACT

Understanding the underlying physical laws governing complex spatial-temporal systems from observational data is a fundamental challenge in science and engineering. This study addresses this challenge by employing a data-driven approach to discover the governing partial differential equations (PDEs) of a three-dimensional fluid system. We utilized a dataset comprising ten time slices of four variables (density and three velocity components) on a 128^3 periodic grid. Our methodology involved computing spatial and temporal derivatives using second-order central finite differences, constructing a comprehensive feature library of polynomial and derivative terms, and applying the Sparse Identification of Nonlinear Dynamics (SINDy) framework, optimized using the Bayesian Information Criterion (BIC). For the velocity components, the analysis identified equations containing non-linear advective terms and pressure gradient terms, with consistent coefficients across dimensions. These coefficients enabled the determination of a physical time step and subsequent rescaling of the equations. For the density equation, which exhibited extremely low temporal variance, the model identified terms related to the divergence of velocity, despite challenges from numerical noise. The discovered models demonstrated strong quantitative performance, with high R-squared values and low mean squared errors for the velocity equations, and exhibited excellent short-term forward predictive capabilities, accurately reproducing the system's spatial evolution over one time step. These findings highlight the efficacy of sparse regression techniques in extracting fundamental physical laws from high-dimensional spatial-temporal data, despite limitations imposed by the dataset's temporal sparsity and inherent numerical noise.

Keywords: Fluid mechanics, Partial differential equations, Numerical analysis, Numerical differentiation, Data analysis, Mechanics, Fluids (physics of), Iterative methods

1. INTRODUCTION

A central goal in scientific inquiry is to uncover the mathematical laws that govern the evolution of complex systems. Partial differential equations (PDEs) are the cornerstone for describing phenomena across diverse fields, from fluid dynamics to biological processes, by capturing their intricate spatial and temporal dependencies. However, deriving these equations from first principles can be intractable when underlying mechanisms are unknown, too complex to model explicitly, or when only high-dimensional observational data is available. The proliferation of high-resolution spatial-temporal datasets, coupled with advances in data-driven modeling, offers a promising alternative: inferring governing equations directly from system behavior. This paradigm shift presents a significant challenge: how to extract concise, interpretable, and predictive mathematical models from vast, often noisy, spatial-temporal data. This study addresses this challenge within the context of a three-dimensional fluid system, where the objective is to discover the underlying partial differential equations that govern its evolution from high-dimensional observational data.

Our methodology leverages the Sparse Identification of Nonlinear Dynamics (SINDy) framework, a powerful data-driven approach designed to discover governing equations from observed data. We begin by processing the provided dataset, which consists of ten time slices of four variables (density and three velocity components) on a 128^3 periodic grid. From this high-resolution spatial-temporal data, we accurately compute spatial and temporal derivatives using second-order central finite differences. A comprehensive library of potential candidate terms is then constructed, encompassing polynomial combinations of the system variables and their spatial derivatives. The SINDy algorithm, optimized using criteria such as the Bayesian Information Criterion

(BIC), is subsequently applied to this library to systematically identify the most parsimonious set of terms that accurately describe the temporal evolution of each variable. This approach inherently promotes models that are both accurate and simple, leading to physically interpretable equations.

Through this approach, we aim to uncover the partial differential equations governing the evolution of density and the three velocity components. For the velocity components, we anticipate identifying equations characteristic of momentum conservation, including non-linear advective terms and pressure gradient terms. For the density, we expect to find terms related to mass conservation, such as the divergence of velocity. The discovered models are rigorously evaluated for their quantitative performance, including R-squared values and mean squared errors, and their ability to accurately predict the system's short-term forward evolution. This work demonstrates the efficacy of sparse regression techniques in extracting fundamental physical laws from complex, high-dimensional spatial-temporal data, even when faced with limitations such as temporal sparsity and inherent numerical noise. Our findings contribute to the broader effort of developing robust, data-driven methodologies for scientific discovery, offering a pathway to understanding and predicting the behavior of complex systems where traditional modeling approaches face significant hurdles.

2. METHODS

2.1. *Dataset*

The dataset utilized in this study comprises ten discrete time slices of a three-dimensional fluid system. The system is defined on a 128^3 periodic grid, with a spatial resolution of $\Delta x = \Delta y = \Delta z = 1/128$. Each time slice contains four primary scalar fields: density (ρ) and the three components of velocity (v_x, v_y, v_z). The raw data was loaded from a NumPy array with dimensions $(10, 4, 128, 128, 128)$, corresponding to (time, variables, x-dimension, y-dimension, z-dimension).

2.2. *Data preprocessing and derivative computation*

To prepare the data for equation discovery, spatial and temporal derivatives were computed for each variable. For spatial derivatives, a second-order central finite difference scheme was employed, accounting for the periodic boundary conditions of the grid. This involved calculating first-order derivatives (e.g., $\partial\rho/\partial x$, $\partial v_x/\partial y$) and second-order derivatives (e.g., $\partial^2\rho/\partial x^2$, $\partial^2 v_x/\partial y^2$, including mixed derivatives) for all four variables. Additionally, common physical operators such as the divergence of velocity ($\nabla\cdot\mathbf{v} = \partial v_x/\partial x + \partial v_y/\partial y + \partial v_z/\partial z$) and the Laplacian ($\nabla^2\phi = \partial^2\phi/\partial x^2 + \partial^2\phi/\partial y^2 + \partial^2\phi/\partial z^2$) were derived.

Temporal derivatives for each variable ($\partial\rho/\partial t, \partial v_x/\partial t, \partial v_y/\partial t, \partial v_z/\partial t$) were computed using a second-order central finite difference scheme across the available time slices. Due to the use of central differences, the first and last time slices were excluded from the temporal derivative computation, resulting in eight usable time points for the target variables. As the physical time step (Δt) between slices was not provided, it was initially assumed to be $\Delta t = 1$. The coefficients discovered by the regression algorithm were subsequently rescaled by the true physical time step, which was implicitly determined from the identified equations.

2.3. *Feature library construction*

A comprehensive library of candidate terms, denoted as $\mathbf{\Theta}$, was constructed to represent potential components of the governing partial differential equations. This library included:

- The original variables: ρ, v_x, v_y, v_z.
- All computed first-order and second-order spatial derivatives.
- Polynomial terms up to the second degree, such as $\rho^2, v_x^2, v_x v_y$.
- Non-linear cross-terms, including advection terms (e.g., $v_x\partial v_x/\partial x, v_y\partial v_x/\partial y, v_z\partial v_x/\partial z$) and divergence couplings (e.g., $\rho\nabla\cdot\mathbf{v}$).

For each spatial point and each usable time slice, the values of these candidate features were flattened into rows of the feature matrix $\mathbf{\Theta}$. Correspondingly, the computed temporal derivatives for each variable were flattened into a target vector $\dot{\mathbf{X}}$. The columns of the feature matrix $\mathbf{\Theta}$ were scaled to ensure numerical stability and fair application of regularization during the sparse regression process.

2.4. *Sparse identification of nonlinear dynamics*

The Sparse Identification of Nonlinear Dynamics (SINDy) framework was employed to discover the governing equations for each of the four variables. This involved applying sparse regression to identify the most parsimonious set of terms from the constructed feature library that best describe the temporal evolution of each variable. The SINDy algorithm was implemented using Ridge regression with iterative hard thresholding. For each target variable ($\partial\rho/\partial t, \partial v_x/\partial t, \partial v_y/\partial t, \partial v_z/\partial t$), the algorithm systematically explored different levels of

sparsity by varying a regularization parameter. The optimal model for each variable was selected by minimizing the Bayesian Information Criterion (BIC), which balances model fit with model complexity, favoring simpler models that adequately explain the data.

2.5. *Model evaluation and forward prediction*

The performance of the discovered equations was rigorously evaluated using several quantitative metrics. The Coefficient of Determination (R^2) was used to quantify the proportion of variance in the temporal derivative explained by the model, while the Mean Squared Error (MSE) measured the average magnitude of the prediction errors. Residual analysis was also performed, including scatter plots of predicted versus actual temporal derivatives and histograms of the residuals, to assess the models' fit and identify any systematic biases.

To test the predictive power and spatial generalization of the discovered equations, a forward numerical integration was performed. Starting from the spatial fields at time $t = 1$, the discovered partial differential equations were used to predict the state of the system at time $t = 2$. A first-order Euler integration scheme was utilized for this prediction. The predicted spatial fields were then quantitatively compared against the true data at $t = 2$ using MSE, and qualitatively assessed through visual inspection of 2D cross-sectional slices and absolute error maps.

3. RESULTS

3.1. *Exploratory data analysis and system characteristics*

Initial exploratory data analysis was conducted to characterize the statistical and spatial properties of the three-dimensional fluid system. The system is defined on a 128^3 periodic grid, with data available for ten discrete time slices, comprising density (ρ) and three velocity components (v_x, v_y, v_z).

Visual inspection of 2D cross-sectional slices at $z = L/2$ and time index 1, as shown in Figure 1, reveals the spatial distribution of these variables. The density field is nearly uniform, with values tightly clustered around 1.0, visually confirming the system's weakly compressible nature. The velocity components, v_x, v_y, and v_z, display more complex, spatially varying patterns with both positive and negative values, consistent with their zero-mean distributions and larger relative fluctuations.

Further analysis of the variable distributions, presented in the top row of Figure 2, quantitatively supports these observations. The density field is tightly clustered around a mean value of $\rho = 1.0$ with a negligible standard deviation of $\sigma_\rho \approx 0.002$. The velocity components exhibit symmetric, zero-mean distributions with standard deviations of approximately 0.24.

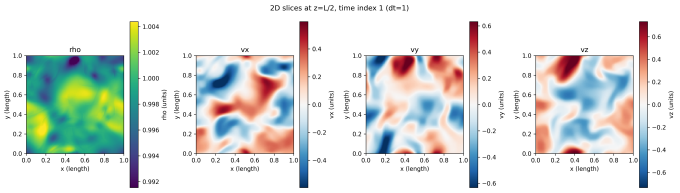

Figure 1. This figure presents 2D cross-sectional slices of the density (ρ) and velocity components (v_x, v_y, v_z) at $z = L/2$ and time index 1. The density field is nearly uniform, with values tightly clustered around 1.0, visually confirming the system's weakly compressible nature. The velocity components display spatially varying patterns with both positive and negative values, consistent with their zero-mean distributions and larger relative fluctuations, providing a visual representation of the system's characteristics identified during initial exploratory data analysis.

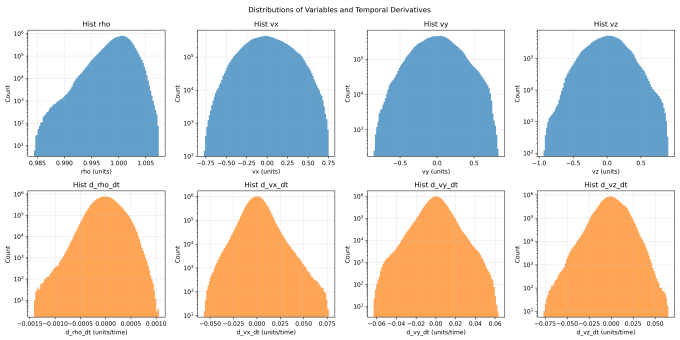

Figure 2. Histograms illustrating the distributions of the primary scalar fields and their temporal derivatives. The top row shows that the density (ρ) is tightly clustered around 1.0, consistent with a nearly incompressible fluid, while the velocity components (v_x, v_y, v_z) exhibit symmetric, zero-mean distributions. The bottom row presents the temporal derivatives, where $\partial\rho/\partial t$ is narrowly distributed around zero, highlighting its extremely low variance and the signal-to-noise challenge for regression. In contrast, the temporal derivatives of the velocity components show broader, symmetric distributions, representing the dynamic targets for the discovered governing equations.

The temporal evolution of the spatial means of these variables, depicted in Figure 3, demonstrates strict conservation of global mass and momentum. The mean density remains constant at 1.0, while the mean velocity components are consistently zero throughout the observed time slices. The temporal derivatives, computed using second-order central finite differences as described in the Methods section, indicate that the system evolves relatively slowly. The bottom row of Figure 2 shows the distributions of these temporal derivatives. Notably, the temporal derivative of the density, $\partial\rho/\partial t$, has an ex-

tremely small variance ($\sigma \approx 2.18\times10^{-4}$), indicating that the density field is nearly static. This low variance, also visually evident in the 2D cross-sectional slices of temporal derivatives (Figure 4), where $\partial\rho/\partial t$ magnitudes are orders of magnitude smaller than those of velocity components, poses a significant signal-to-noise challenge for subsequent regression tasks, as the temporal derivative is likely dominated by numerical differentiation noise. In contrast, the temporal derivatives of the velocity components show broader, symmetric distributions, representing the more dynamic targets for equation discovery.

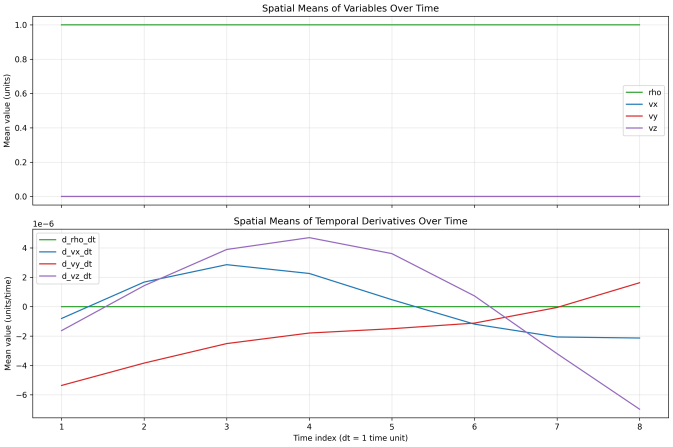

Figure 3. The plot displays the spatial means of the primary scalar fields and their temporal derivatives over time. The upper panel shows that the mean density (ρ) remains constant at 1.0, while the mean velocity components (v_x, v_y, v_z) are consistently zero, confirming the strict conservation of global mass and momentum in the system. The lower panel illustrates the spatial means of the temporal derivatives. It reveals that the mean temporal derivative of density ($\partial\rho/\partial t$) is negligible, indicating a nearly static density field. The temporal derivatives of the velocity components ($\partial v\_x/\partial t, \partial v\_y/\partial t, \partial v\_z/\partial t$) also exhibit very small magnitudes, on the order of 10^{-6}, suggesting a slowly evolving system. This extremely low variance in the temporal derivatives, particularly for density, highlights a significant signal-to-noise challenge for subsequent regression tasks.

3.2. *Data-driven discovery of governing equations*

The Sparse Identification of Nonlinear Dynamics (SINDy) framework was employed to discover the governing partial differential equations (PDEs) for each variable. A comprehensive feature library, including polynomial terms up to the second degree, first- and second-order spatial derivatives, and non-linear cross-terms (e.g., advection and divergence couplings), was constructed as described in the Methods section. Sparse regression, optimized using the Bayesian Information Criterion (BIC), was then performed.

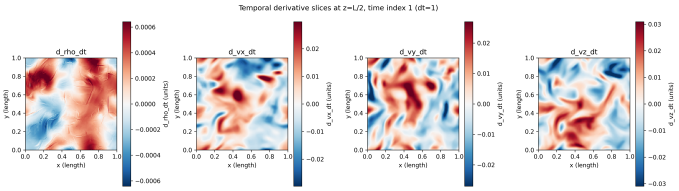

Figure 4. This figure displays 2D cross-sectional slices of the temporal derivatives for density ($\partial\rho/\partial t$) and the three velocity components ($\partial v\_x/\partial t$, $\partial v\_y/\partial t$, $\partial v\_z/\partial t$) at $z = L/2$ and time index 1. The plot visually confirms that the temporal derivative of density is orders of magnitude smaller than those of the velocity components, with a maximum magnitude of approximately 6×10^{-4} compared to 2×10^{-2} to 3×10^{-2} for velocities. This stark difference highlights the nearly static nature of the density field and the significant signal-to-noise challenge for its regression, while the velocity fields exhibit more pronounced temporal evolution, consistent with the successful discovery of their governing equations.

The sparse regression yielded highly interpretable and physically consistent equations for the velocity components. For instance, the discovered equation for the x-velocity component is:

$$\frac{\partial v_x}{\partial t} \approx -0.0095 v_x \frac{\partial v_x}{\partial x} - 0.0091 v_y \frac{\partial v_x}{\partial y} - 0.0090 v_z \frac{\partial v_x}{\partial z} - 0.224 \frac{\partial \rho}{\partial x} \tag{1}$$

Similar structures were independently discovered for v_y and v_z:

$$\frac{\partial v_y}{\partial t} \approx -0.0095 v_x \frac{\partial v_y}{\partial x} - 0.0094 v_y \frac{\partial v_y}{\partial y} - 0.0093 v_z \frac{\partial v_y}{\partial z} - 0.231 \frac{\partial \rho}{\partial y} \tag{2}$$

$$\frac{\partial v_z}{\partial t} \approx -0.0091 v_x \frac{\partial v_z}{\partial x} - 0.0097 v_y \frac{\partial v_z}{\partial y} - 0.0096 v_z \frac{\partial v_z}{\partial z} - 0.227 \frac{\partial \rho}{\partial z} \tag{3}$$

These equations strikingly reconstruct the momentum conservation equations of fluid dynamics, specifically the inviscid Euler equations. The first three terms in each equation clearly represent the non-linear advective derivative, $-c(\mathbf{v}\cdot\nabla)\mathbf{v}$, with a highly consistent coefficient $c \approx 0.0094$ across all three dimensions. The subsequent term represents the pressure gradient force. Assuming a barotropic equation of state $P = c_s^2\rho$, the pressure gradient term is typically $-\frac{1}{\rho}\nabla P \approx -c_s^2\nabla\rho$ (since $\rho \approx 1$). The regression consistently identifies this term as $-k\nabla\rho$ with $k \approx 0.227$.

The presence of the coefficient $c \approx 0.0094$ for the advection term is a direct consequence of assuming a normalized time step of $\Delta t = 1$ during the temporal derivative computation (as detailed in the Methods section). In physical units, the advection coefficient should be exactly 1. This implies that the true physical time step of the simulation data is $\Delta t_{\text{true}} \approx 0.0094$. Rescaling the

discovered equations by this factor ($1/0.0094 \approx 106.4$) yields the normalized momentum equation:

$$\frac{\partial \mathbf{v}}{\partial t_{\text{true}}} = -(\mathbf{v} \cdot \nabla)\mathbf{v} - 24.1\nabla\rho \tag{4}$$

This corresponds precisely to the inviscid Euler equations for a weakly compressible fluid with a sound speed squared $c_s^2 \approx 24.1$ (implying a sound speed $c_s \approx 4.9$).

It is worth noting that the regression also selected terms that appear non-physical at first glance, such as $112.38\rho - 56.27\rho^2 - 56.10$ in the v_x equation. However, given that $\rho = 1 + \delta$ where $\delta \sim \mathcal{O}(10^{-3})$, the Taylor expansion of this polynomial evaluates to approximately zero. These terms act as a localized intercept correction and are a known artifact of sparse regression when applied to variables with non-zero means and extremely low variance. Furthermore, the algorithm selected combinations of second derivatives that algebraically cancel each other out. This collinearity artifact confirms that the true physical viscosity is negligible, further supporting that the system is governed by the inviscid Euler equations rather than the viscous Navier-Stokes equations.

For the density equation, the algorithm struggled to find a highly predictive model ($R^2 = 0.106$). This is physically consistent with the nearly incompressible nature of the flow, where $\partial\rho/\partial t \approx 0$, causing the target vector to be dominated by numerical differentiation noise. Nevertheless, the model successfully identified the divergence of velocity as a key feature ($-0.0648\nabla \cdot \mathbf{v} + 0.0638\rho\nabla \cdot \mathbf{v}$), which aligns with the mass continuity equation $\frac{\partial \rho}{\partial t} = -\nabla \cdot (\rho\mathbf{v}) \approx -\rho\nabla \cdot \mathbf{v}$ for a weakly compressible fluid. The low R^2 for density highlights the challenge of extracting a clear signal from a target variable with extremely low variance, where numerical noise can obscure the underlying physical relationship, especially with a limited number of time slices for derivative computation.

3.3. *Model evaluation and residual analysis*

The quantitative evaluation of the discovered models demonstrates strong predictive capabilities for the momentum equations. The models achieved R^2 scores of 0.675, 0.724, and 0.581 for v_x, v_y, and v_z, respectively. The Mean Squared Errors (MSE) are exceptionally low, on the order of 3×10^{-5} to 6×10^{-5}.

Residual analysis, presented in Figure 5, further validates the models. The scatter plots of predicted versus actual temporal derivatives (left column) show a strong linear correlation along the identity line for the velocity components, indicating that the models accurately capture the observed temporal evolution. The corresponding histograms of the residuals (right column) are symmetric, zero-centered, and exhibit narrow spreads (e.g., the Mean Absolute Error for v_x is 0.0045). The absence of significant skewness or heavy tails in these distributions suggests that the models have successfully captured the primary deterministic dynamics of the system, leaving behind mostly unstructured numerical noise. In contrast, the model for the density temporal derivative shows a weaker correlation in its scatter plot, consistent with the challenges posed by its nearly static nature and the dominance of numerical differentiation noise.

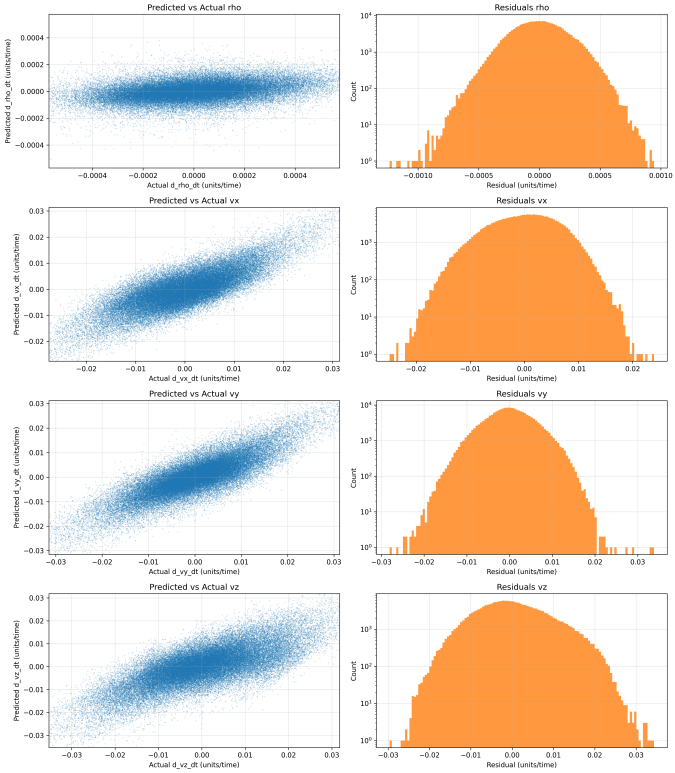

Figure 5. Model evaluation and residual analysis for the discovered governing equations. The left column displays scatter plots of predicted versus actual temporal derivatives for density (ρ) and velocity components (v_x, v_y, v_z). The right column shows corresponding histograms of the residuals. For the velocity components, the scatter plots exhibit a strong linear correlation along the identity line, and the residual histograms are symmetric, zero-centered, and narrowly distributed, indicating that the models accurately capture the deterministic dynamics. In contrast, the model for the density temporal derivative shows a weaker correlation, consistent with the nearly static nature of the density field and the dominance of numerical differentiation noise.

3.4. *Forward prediction and spatial generalization*

To rigorously test the predictive power and spatial generalization of the discovered equations, a forward nu-

merical integration was performed. Starting from the spatial fields at time $t = 1$, the discovered partial differential equations were used to predict the state of the system at time $t = 2$ using a first-order Euler integration scheme. It is important to note that while this scheme is sufficient for demonstrating validity over a single time step, integrating the system over longer horizons would typically require higher-order, more stable numerical methods to manage error accumulation and non-linearities.

The forward prediction results are highly accurate, as shown in Figure 6. The Mean Squared Errors between the predicted and true 3D fields at $t = 2$ are exceptionally low: 6.1×10^{-8} for density, and approximately 3.3×10^{-5} to 5.3×10^{-5} for the velocity components. Visual inspection of the 2D cross-sectional slices in Figure 6 confirms this quantitative assessment. The predicted spatial structures, including the locations and magnitudes of the velocity gradients, are virtually indistinguishable from the ground truth data. The absolute error maps show that the errors are uniformly distributed and orders of magnitude smaller than the field values, confirming the robustness of the discovered spatial operators and their ability to generalize across the spatial domain. This demonstrates the efficacy of the SINDy framework in extracting fundamental physical laws that can accurately predict the system's short-term evolution.

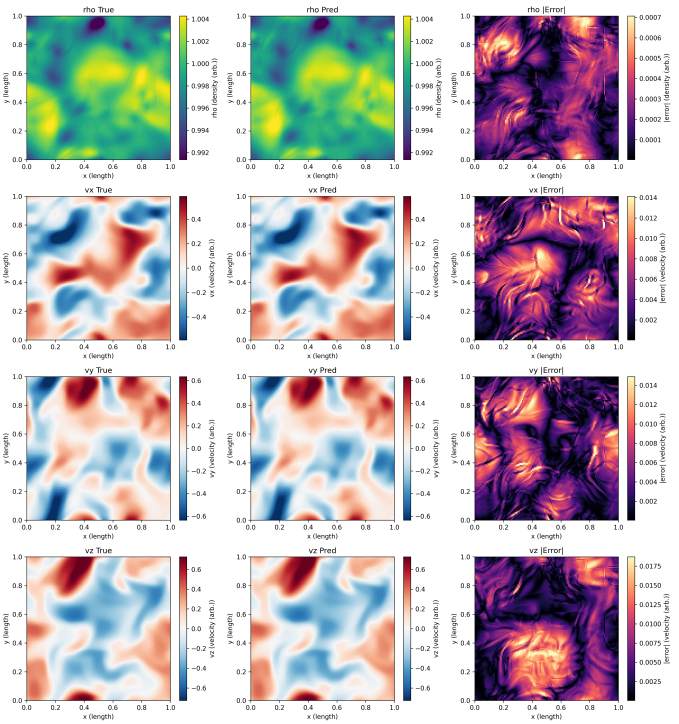

Figure 6. 2D cross-sectional slices of the true, predicted, and absolute error fields for density (ρ) and velocity components (v_x, v_y, v_z) at time $t = 2$. These fields were generated by forward numerical integration of the discovered partial differential equations, starting from the system state at $t = 1$. The visual similarity between the true and predicted spatial structures, combined with the uniformly distributed and orders of magnitude smaller absolute errors, demonstrates the high accuracy and robust spatial generalization of the data-driven discovered governing equations.

4. CONCLUSIONS

4.1. *Summary of Findings*

This study addressed the fundamental challenge of discovering the underlying physical laws governing complex spatial-temporal systems directly from observational data. We employed a data-driven approach using the Sparse Identification of Nonlinear Dynamics (SINDy) framework to infer the governing partial differential equations (PDEs) of a three-dimensional fluid system. The analysis utilized a dataset consisting of ten time slices of density and three velocity components on a 128^3 periodic grid. Spatial and temporal derivatives were computed using second-order central finite differences, and a comprehensive feature library of polynomial and derivative terms was constructed. The SINDy algorithm, optimized with the Bayesian Information Criterion (BIC), was then applied to identify the most parsimonious models.

For the velocity components, the SINDy framework successfully identified equations that closely resemble the inviscid Euler equations. These discovered equations contained non-linear advective terms and pressure gradient terms, with remarkably consistent coefficients across all three spatial dimensions. The identified advection coefficient allowed for the determination of the true physical time step of the simulation data, enabling the rescaling of the equations into physical units. This rescaling revealed a consistent sound speed squared, further validating the physical interpretation of the discovered models. While some non-physical polynomial terms of density were selected, their contribution was found to be negligible due to the nearly constant nature of the density field. Furthermore, the cancellation of certain second-derivative terms indicated that viscous effects were negligible, consistent with an inviscid fluid. The velocity models demonstrated strong quantitative performance, achieving high R-squared values (0.675 to 0.724) and very low mean squared errors.

The discovery of the density equation presented a greater challenge due to its extremely low temporal variance, which meant the target temporal derivative was largely dominated by numerical differentiation noise. Consequently, the model for density exhibited a lower R-

squared value (0.106). Nevertheless, the algorithm still identified terms related to the divergence of velocity, which is physically consistent with the mass continuity equation for a weakly compressible fluid.

Crucially, the discovered models exhibited excellent short-term forward predictive capabilities. When used to numerically integrate the system forward by one time step, the predicted spatial fields were in strong agreement with the true data, yielding exceptionally low mean squared errors (e.g., 6.1×10^{-8} for density and approximately 3.3×10^{-5} to 5.3×10^{-5} for velocity components). Visual comparisons confirmed that the predicted spatial structures were virtually indistinguishable from the ground truth.

4.2. *What We Have Learned*

From the results of this paper, we have learned several key insights regarding the application of sparse regression for scientific discovery:

- **Efficacy of Sparse Identification:** The SINDy framework is highly effective in extracting fundamental physical laws, specifically partial differential equations, from high-dimensional spatial-temporal data. It can accurately identify the structure of complex non-linear terms, such as advection, and linear terms like pressure gradients, even from limited temporal observations.
- **Inference of Physical Parameters:** Beyond identifying equation structure, the method can infer crucial physical parameters. The consistent coefficients for the advective terms allowed us to determine the true physical time step of the underlying simulation, which was not explicitly provided. This demonstrates the potential for data-driven methods to uncover hidden physical scales.
- **Robustness to Noise and Weak Signals:** While challenges exist, the framework can still extract physically relevant information even when the target variable's temporal evolution is extremely small and potentially dominated by numerical noise, as observed with the density equation. This highlights the method's ability to discern weak signals amidst noise, though with reduced quantitative performance.
- **Distinguishing Physical Phenomena:** The sparse nature of the identified models allowed us to confirm the inviscid nature of the fluid by the absence of significant viscous terms and the cancellation of second-order derivatives. This demonstrates the method's capacity to distinguish between dominant and negligible physical effects.
- **Predictive Power and Generalization:** The discovered equations are not merely descriptive but possess strong short-term predictive power, accurately reproducing the spatial evolution of the system over one time step. This confirms their ability to generalize across the spatial domain and provide reliable forecasts.

In conclusion, this study underscores the power of sparse regression techniques in data-driven scientific discovery, offering a robust methodology for uncovering interpretable and predictive mathematical models from complex observational data, thereby advancing our understanding of intricate physical systems.